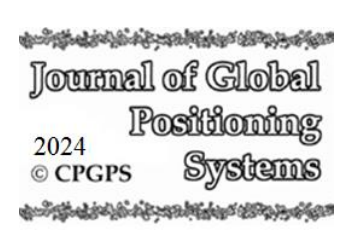
DOI:10.5081/jgps.20.1.13



# Double layer dynamic target capture algorithm based on improved EKF and GBNN

Qian Sun<sup>1,2,⊠</sup>, Xingyu Zhou<sup>1,2</sup>, Weiyang Zhao<sup>1,2</sup>, Xing Jian<sup>1,2</sup>

- 1, College of Information and Communication Engineering, Harbin Engineering University, Harbin 150001, China
- 2, The Key Laboratory of Advanced Marine Communication and Information Technology, Harbin 150001, China

Email: <u>qsun@hrbeu.edu.cn</u>

Abstract: To address the challenges of energy constraints, high real-time requirements, and strong adversarial conditions in underwater dynamic target pursuit tasks, a highly efficient two-layer dynamic target pursuit algorithm is proposed to overcome the limitations of multi-autonomous underwater vehicle systems in terms of coordination efficiency and task execution. First, by analyzing the relative velocities of pursuers and the target, the Apollonius circle principle is extended to three-dimensional space, facilitating a pursuit strategy that aligns more effectively with real-world underwater conditions. Second, to mitigate the inherent measurement errors of sonar detection systems, an adaptive Kalman filter is designed to effectively suppress noise interference and achieve real-time, accurate prediction of the target AUV's motion trajectory. Furthermore, by reconstructing the neuronal activity propagation mechanism of the Glasius bio-inspired neural network, the collaborative decision-making process of multiple AUVs is optimized, significantly enhancing task execution efficiency. Simulation results demonstrate that the proposed algorithm improves pursuit distance and time by at least 30% and 24%. respectively. In multi-scenario generalization tests, the average pursuit distance and time are improved by at least 25% and 18%, respectively. In anti-interference tests under varying sonar detection accuracies, the average pursuit distance and time are enhanced by at least 25% and 22%, respectively. These results collectively validate the superior accuracy, robustness, and adaptability of the proposed algorithm.

**Key words**: Dynamic target capture, Adaptive Kalman filter, Glasius bio-inspired neural network, Apollonius circle.

## I. INTRODUCTION

Autonomous Underwater Vehicle (AUV) is an unmanned underwater robot that is increasingly important in ocean exploration and military applications due to its small size, low cost, stealthy nature, and high flexibility. AUVs are not affected by the weather and capable of performing tasks such as cooperative search<sup>[1-3]</sup>, target tracking<sup>[4-6]</sup>, and cooperative encirclement<sup>[7-9]</sup> over extended durations. Among numerous applications, dynamic target capture is a challenging task, which has gained significant development on unmanned platforms in recent years as a fundamental component of path planning. Based on the solution approach, algorithms for solving the dynamic target rounding problem can be categorized into force-based algorithms, learning-based algorithms, and bio-inspired algorithms.

Force-based algorithms<sup>[10,11]</sup> treat the target as a gravitational source generating an attractive force to guide pursuers toward it, while treating obstacles as repulsive sources to prevent collisions. The method is easy to implement and can respond quickly to dynamic changes. Although these algorithms produce collision-free paths, they are often suboptimal and computationally demanding in complex environments with numerous obstacles, hindering real-time performance.

In learning-based algorithms, AUVs are regarded as intelligences that acquire rewards through trial and error in the process of interacting with the environment, and gradually learn optimal action strategies<sup>[12]</sup>. This data-driven approach allows the algorithm to dynamically adjust its strategy to the uncertainties and changes in the underwater mission by learning the feedback from the environment, but its training cost is too high and the model may fail due to data bias or noise interference in extreme or untrained environments.

In bio-inspired algorithms, the cooperative pursuit problem is often considered as a modification of group behavior. In recent years, Bio-inspired Neural Networks (BINN) and their variant, Glasius Bio-inspired Neural Networks (GBNN), have attracted significant attention in the field of multi-intelligence due to their efficiency and flexibility. BINN as a real-time planning algorithm, the updating process is computationally burdensome; while GBNN reduces the computational complexity, but the information propagation delay may still cause it to fall into a local optimal solution [13].

The existing literature has extensively explored methods for dynamic target encirclement, yet several shortcomings remain. First, most studies are confined to two-dimensional planes and neglect the influence of ocean currents. In highly adversarial scenarios such as dynamic target encirclement, depth variations and ocean current effects are critical factors that cannot be overlooked. Therefore, investigating three-dimensional dynamic encirclement under the influence of ocean currents holds significant practical importance. Second, current algorithms typically assume precise knowledge of the target's position, ignoring the impact of sonar detection accuracy on encirclement efficiency, which deviates significantly from real-world conditions.

To address these issues, this paper proposes a duallayer dynamic target encirclement algorithm that integrates an improved Extended Kalman Filter (EKF) with an enhanced GBNN. The algorithm analyzes the velocity relationship between the pursuing AUVs and the target, incorporating the Apollonius Circle theory to extend the encirclement process into threedimensional space. The improved EKF effectively mitigates the impact of sonar detection inaccuracies, enabling precise prediction of the target AUV's position at the next time step. Additionally, by integrating ocean current information into the enhanced GBNN and optimizing the propagation mechanism of neuron activation values, the algorithm significantly improves its ability to escape local dead zones, thereby achieving rapid and robust encirclement of dynamic targets by multiple AUVs.

#### II. RELATED WORK

#### 1. Problem modeling

In this paper, we study the process of executing a cooperative capture task under the influence of ocean currents by an intelligent cluster of multiple homogeneous AUVs in a three-dimensional underwater environment. In this environment, there are multiple static obstacles. The rounding AUVs attempt to round up a target with intelligent countermeasure capabilities, which dynamically adjusts its movement strategy according to the level of threat it faces. At the beginning of the mission, the rounding AUV starts from an initial position and

gradually approaches the target, eventually realizing its encirclement. When the enemy target does not detect the AUV, it moves randomly at cruising speed; once it detects the AUV, it will escape at a higher speed and intelligently selects an escape mode based on predefined escape rules.

#### 1.1 Simplified AUV model

Define the state vector of the smart body as  $[x_i, y_i, z_i, \theta_i, \varphi_i]$ , where  $x_i, y_i, z_i$  are the coordinates of the *i*-th AUV in the geodetic coordinate system, and  $\theta_i, \varphi_i$  are the pitch angle and yaw angle of the *i*-th AUV, respectively. Meanwhile, the horizontal and vertical rotation rates are defined as  $\omega_i$  and  $\phi_i$  as the control inputs of the *i*-th AUV, respectively. Therefore, the continuous kinematic model can be defined as follow

$$\begin{cases} \dot{x}_i = v_i \cos \varphi_i \cos \theta_i \\ \dot{y}_i = v_i \cos \varphi_i \sin \theta_i \\ \dot{z}_i = v_i \sin \varphi_i \end{cases}$$

where  $v_i$  is the sailing speed of the *i*-th AUV. As a result, the kinematic model of the next time step of the AUV [14] can be described as

$$\begin{cases} x_i^{t+1} = x_i^t + v_i^t \cos(\varphi_i^t + \phi_i^t \Delta t) \cos(\theta_i^t + \omega_i^t \Delta t) \cdot \Delta t \\ y_i^{t+1} = y_i^t + v_i^t \cos(\varphi_i^t + \phi_i^t \Delta t) \sin(\theta_i^t + \omega_i^t \Delta t) \cdot \Delta t \\ z_i^{t+1} = z_i^t + v_i^t \sin(\varphi_i^t + \phi_i^t \Delta t) \cdot \Delta t \end{cases}$$
(2)

where the superscript t indicates the current time and the sampling interval is a time step.

#### 1.2 Environment model

AUVs are affected by ocean currents when performing dynamic target roundup missions. Considering that the mission area is in deeper waters, the current speed is usually low. Therefore, the current speed in the longitudinal direction can be ignored. However, the current in the grid where the AUV is located still affects its navigation speed and thus its time to reach the target location<sup>[15]</sup>. The ocean flow in the mission environment is formed by the superposition of several two-dimensional Navier-Stokes equations as shown in the following equation

$$V_{e,x} = -\frac{\Omega_{e} \left( y - y_{e} \right)}{2\pi \left| \boldsymbol{\chi} - \boldsymbol{\chi}_{e} \right|_{2}^{2}} \cdot \left( 1 - \exp \left( -\frac{\left| \boldsymbol{\chi} - \boldsymbol{\chi}_{e} \right|_{2}^{2}}{r_{e}^{2}} \right) \right)$$

$$V_{e,y} = -\frac{\Omega_{e} \left( x - x_{e} \right)}{2\pi \left| \boldsymbol{\chi} - \boldsymbol{\chi}_{e} \right|_{2}^{2}} \cdot \left( 1 - \exp \left( -\frac{\left| \boldsymbol{\chi} - \boldsymbol{\chi}_{e} \right|_{2}^{2}}{r_{e}^{2}} \right) \right)$$
(3)

(4)

where  $V_c = (V_{cx}, V_{cy})$  represents the current vector at the point  $\chi = (x, y)$ ,  $\chi_c = (x, y_c)$  denotes the center of the

Lamb vortex, and  $\Omega_c$ ,  $r_c$  are the intensity and radius of the vortex, respectively.

#### 1.3 Apollonius circle decision model

Each AUV is constrained in its ability to maneuver due to overload limitations, and the maximum area it can reach is referred to as the containment area. Similarly, the escape boundary of a target is the area that can be reached by the target while performing escape maneuvers with maximum overload. If the AUV's roundup zone can completely cover the target's escape boundary, the roundup is considered to be successful. Therefore, effective roundup of the target can be realized by multiple AUVs cooperating to form a larger roundup area. The schematic diagram of the principle is shown below [16][17].

For a single AUV, the Apollonius circle delineates its capture region based on the target's position and velocity. The position coordinates of the enclosing AUV are  $[x_a, y_a, z_a]$ , the coordinates of the target AUV are  $[x_{tar}, y_{tar}, z_{tar}]$ , and let the coordinates of the encounter point P be [x, y, z], and the ratio of the distance of the point P to the enclosing AUV and the target AUV is a constant k

$$k = \frac{\sqrt{(x - x_a)^2 + (y - y_a)^2 + (z - z_a)^2}}{\sqrt{(x - x_{tar})^2 + (y - y_{tar})^2 + (z - z_{tar})^2}}$$

When k=1, the trajectory of point P is a branch of the hyperbola, and when  $k \neq 1$ , the trajectory is the Apollonius circle. Introduced into the enclosure problem, assuming that a time step in the AUV and target axial motion velocity size constant, the encounter point P to reach the two distance ratio

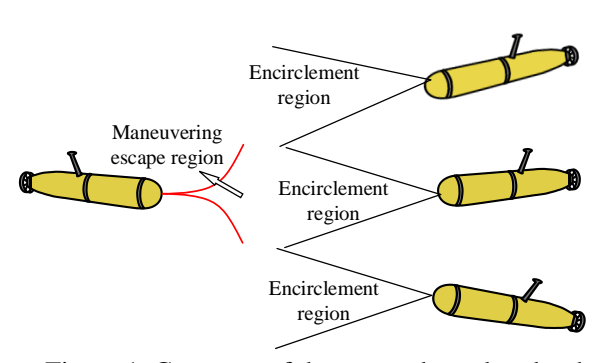


Figure 1. Coverage of the escape boundary by the capture area

that is the ratio of speed, for  $k = v_a / v_{tar}$ , that is, the AUV on the target of the enclosure space that is the encounter point P trajectory formed by the Apollonius circle, the relevant parameters with the AUV and the target's speed, which  $v_a$  is the enclosure of the AUV's speed size,  $v_{tar}$  is the size of the target's speed. The center A  $(x_A, y_A, z_A)$  and

radius of the Apollonius circle  $r_{Ap}$  can be calculated based on the position of the AUV and the target and the velocity ratio, and the formula is as follows

$$(x_A, y_A, z_A) = \left(\frac{x_a - k^2 x_{tar}}{1 - k^2}, \frac{y_a - k^2 y_{tar}}{1 - k^2}, \frac{z_a - k^2 z_{tar}}{1 - k^2}\right)$$

$$r_{Ap} = \frac{k\sqrt{(x_a - x_{tar})^2 + (y_a - y_{tar})^2 + (z_a - z_{tar})^2}}{|1 - k^2|}$$

(6)

The core idea of multi-AUV cooperative roundup is to use the combination of multiple Apollonius circles to construct a roundup area that can completely cover the escape area of the target AUV, so as to realize the success of roundup. And in the 3D rasterized environment, the sign of successful roundup is that all the target points that the target may escape to in the next time step, i.e., the neighboring raster with the resolution of sailing distance of one-time step centered on itself, are all included in the combined area of Apollonios spheres formed by multiple AUVs.

#### 2. Dynamic target rounding algorithm

#### 2.1 IEKF algorithm

Based on the AUV kinematic model in (2), the state transfer process is described a

$$X(k) = f(X(k-1), c(k-1))$$
(7)

Where, k denotes any sampling moment, X(k) denotes the state vector of the AUV at the moment k, and c(k-1) denotes the control input at the moment  $k-1^{[18]}$ .

The observation quantity is  $\mathbf{Z}(k) = [d_i, \alpha_i, \beta_i]$ , which is the distance of the target from the device, the yaw angle and the pitch angle measured by the device at the time step. By establishing the state transfer equation and observation equation of the AUV, the EKF is able to describe the movement pattern of the AUV at each time step and its relationship with the observation data. Among them, the observation equation can be described in the following form

$$Z(k) = h[X(k | k-1)]$$
(8)

$$h[X(k)] = \begin{bmatrix} \sqrt{(x_{k} - x_{0})^{2} + (y_{k} - y_{0})^{2} + (z_{k} - z_{0})^{2}} \\ \tan^{-1}(\frac{y_{k} - y_{0}}{x_{k} - x_{0}}) \\ \tan^{-1}(\frac{z_{k} - z_{0}}{\sqrt{(x_{k} - x_{0})^{2} + (y_{k} - y_{0})^{2}}}) \end{bmatrix}$$

where h[X(k)] is a nonlinear function of state to observation.  $x_0, y_0, z_0$  is the coordinates of the

observatory set to 0, 0, 0,  $x_k$ ,  $y_k$ ,  $z_k$  is the coordinates of the location of the AUV at the time.

To mitigate the impact of outliers on prediction accuracy, the results are smoothed using an Exponential Moving Average (EMA).

$$\mathbf{Z}_{EMA}(k) = (1 - \delta) \cdot \mathbf{Z}(k) + \delta \cdot \mathbf{Z}_{EMA}(k - 1)$$
10)

where,  $\mathbf{Z}_{\text{EMA}}(k)$  is the smoothed value of the moment k,  $\mathbf{Z}(k)$  is the observed value of the moment,  $\delta$  is the smoothing coefficient, Based on expert experience<sup>[19]</sup>, its value should be between 0.9 and 1, and the smaller the value of the more inclined to recent observations, the larger the value of the smoothing effect is stronger.

One-step state prediction of the target after obtaining the observations

$$\begin{cases} \hat{\boldsymbol{X}}(k \mid k-1) = \boldsymbol{F} \cdot \hat{\boldsymbol{X}}(k-1) \\ \boldsymbol{P}(k \mid k-1) = \boldsymbol{F} \cdot \boldsymbol{P}(k-1) \cdot \boldsymbol{F}^T + \boldsymbol{Q}(k) \end{cases}$$
11)

where  $\hat{X}(k-1)$  is the state estimate at the previous moment, F is the state transfer matrix, which is the partial differential Jacobi matrix of the state transfer equation f(X(k-1),c(k-1)), P(k-1) is the state covariance matrix at the previous moment, which represents the error range of the state estimate, and Q(k) is the process noise covariance matrix at the time, which represents the uncertainty due to the unmodeled dynamics in the model<sup>[20]</sup>.

The update process follows:

$$\begin{cases} \boldsymbol{K}(k) = \\ \boldsymbol{P}(k \mid k-1) \cdot \boldsymbol{H}^{T}(k) \cdot [\boldsymbol{H}(k)\boldsymbol{P}(k \mid k-1)\boldsymbol{H}^{T}(k) + \boldsymbol{R}(k)]^{-1} \\ \hat{\boldsymbol{X}}(k) = \hat{\boldsymbol{X}}(k \mid k-1) + \boldsymbol{K}(k) \cdot [\boldsymbol{Z}_{EMA}(k) - \hat{\boldsymbol{Z}}_{EMA}(k)] \\ \boldsymbol{P}(k) = [\boldsymbol{I} - \boldsymbol{K}(k)\boldsymbol{H}(k)]\boldsymbol{P}(k \mid k-1) \end{cases}$$

(12)

where P(k | k-1) is the predicted covariance matrix, R(k) is the time-observed noise covariance matrix  $I^{[21]}$ , the Jacobi matrix  $I^{[21]}$ , denotes the first-order partial derivatives with respect to  $I^{[21]}$ , and  $I^{[21]}$  is the unit matrix. The updating process of  $I^{[21]}$  and  $I^{[21]}$  with is as follows

$$\begin{cases} \mathbf{R}(k) = (1 - \gamma)\mathbf{R}(k - 1) + \gamma(\mathbf{\varepsilon}_k \mathbf{\varepsilon}_k^T - \mathbf{H}_k \mathbf{P}(k \mid k - 1)\mathbf{H}_k^T) \\ \mathbf{Q}(k) = (1 - \lambda)\mathbf{Q}(k - 1) + \lambda(\mathbf{\varepsilon}_k \mathbf{\varepsilon}_k^T) \end{cases}$$

(13)

where  $\varepsilon_k$  is the innovation series, which measures the deviation between forecasts and actual observations.  $\gamma$  is an adaptive weighting factor,  $\lambda$  is an updating

factor  $(0 \le \lambda \le 1)^{[22][23]}$ , and the relevant parameters are as follows

$$\begin{cases} \boldsymbol{\varepsilon}_{k} = \mathbf{Z}_{EMA}(k) - h(\hat{\boldsymbol{X}}(k \mid k - 1)) \\ \gamma = \frac{1 - \rho}{1 - \rho^{k}} \end{cases}$$
(14)

where  $h(\hat{X}(k \mid k-1))$  is the observed value obtained from the prediction and  $\rho$  is the scaling factor  $(0.95 \le \rho \le 0.99)^{[24][25]}$ . The settings of  $\rho$  and  $\lambda$  directly affect the update speed of R(k) and Q(k). A smaller update speed can make adjustments smoother, reducing the instability of the Kalman gain caused by rapid changes in R(k) and Q(k).

The whole prediction and updating process of IEKF is shown in Figure 2. This method avoids the limitations of the traditional EKF that relies too much on the number of observations and static noise settings, and allows the filter to adaptively adjust to the real-time performance of the system, thus providing more accurate state estimation.

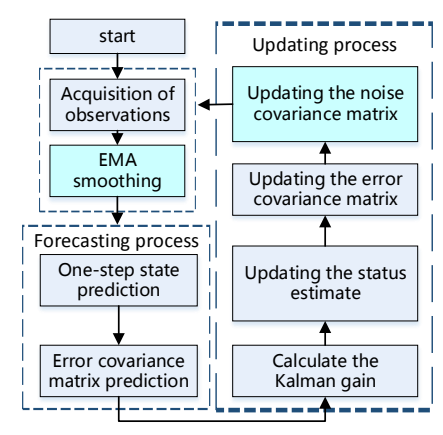


Figure 2. IEKF's prediction and update process

#### 2.2 IGBNN algorithm

This study analyzes the GBNN updating process to enhance the search efficiency of individual AUVs by enhancing the global information dissemination mechanism as well as improving the effectiveness of external stimuli.

The GBNN consists of discrete Hopfield neurons. In the 3D GBNN model, each neuron corresponds to a discrete lattice in the configuration space and is connected to only 26 neurons in its neighborhood, which is considered as a spherical region of radius  $r_{\rm sen}$ , the receptive field of the neuron [26]. The weight of the connection between the neuron m and the neuron n is shown in the following equation:

$$W_{m,n} = \begin{cases} \exp(-\eta |\boldsymbol{p}_{m} - \boldsymbol{p}_{n}|_{2}), |\boldsymbol{p}_{m} - \boldsymbol{p}_{n}|_{2} \leq r_{\text{sen}} \\ 0, & |\boldsymbol{p}_{m} - \boldsymbol{p}_{n}|_{2} > r_{\text{sen}} \end{cases}$$
(15)

where  $|\boldsymbol{p}_{\scriptscriptstyle m}-\boldsymbol{p}_{\scriptscriptstyle n}|_2$  is the Euclidean distance between two neurons,  $\eta>0$  is the attenuation factor<sup>[27]</sup>, and the connection weight  $w_{\scriptscriptstyle m,n}$  is responsible for the delay and attenuation of the information propagation, and the connection between neighboring neurons is the key to the propagation of global information by the GBNN

From the point of view of a single neuron,  $a_m^{\text{rel}}$  is the dynamic output of the neuron m, also known as the neuron's activity value, is shown in the following equation

$$a_{m}^{t+1} = g\left(I_{m}^{t} + \sum_{n \in N(m)} w_{m,n} \cdot a_{n}^{t}\right)$$

(16)

where N(m) is the set of neurons within the receptive field of the m-th neuron,  $g(\square)$  is the transformation function, and  $I_m'$  is the external stimulus received by the m-th neuron at moment t. In the GBNN model, stimuli usually include inhibitory stimuli and excitatory stimuli. Excitatory stimuli are related to the relative positions of the encloser and the target. Meanwhile, grids that do not meet the problem constraints, such as those occupied by obstacles, produce inhibitory stimuli as follows

$$I'_{m} = \begin{pmatrix} e & \text{m is target} \\ -e & \text{m is obstacle} \\ 0 & \text{others} \end{pmatrix}$$

(17)

$$g(a) = \begin{cases} 0 & a < 0 \\ \beta a & 0 \le a \le 1 \\ 1 & a > 1 \end{cases}$$

(18)

where e is a constant much larger than 1. The transformation function g(a) causes the activity value to decrease in an orderly fashion with transmission and  $0 < \beta < 1$  is constant [28].

In the GBNN model, global information with the target location is propagated through the connections between neurons, and this unique propagation mechanism embeds the global information into the neighborhood reward of the GBNN, which enables it to select a more optimal waypoint. However, the propagation of information in the GBNN model suffers from time delay and decay, and the dynamic output computation of the neurons may also lead to their tendency to fall into local optimal solutions. For this reason, in this section, improvements are made in terms of both the propagation process and external stimuli, aiming to enhance the model's ability to jump out of the local optimal solution, and thus improve the performance of a single AUV in a roundup mission.

When performing a roundup mission, it will be affected by ocean currents, which will change the sailing speed and ultimately affect the roundup efficiency. When performing the roundup task, the current markers on the GBNN network must be taken into account<sup>[29]</sup>, and the formula for the connection weights can be rewritten as

$$W_{m,n} = \begin{cases} \exp\left(-\frac{\eta \left|\boldsymbol{p}_{m} - \boldsymbol{p}_{n}\right|_{2}}{\left|\hat{\boldsymbol{V}}_{a}^{m \to n}\right|_{2}}\right), & \left|\boldsymbol{p}_{m} - \boldsymbol{p}_{n}\right|_{2} \leq r_{\text{sen}} \\ 0, & \left|\boldsymbol{p}_{m} - \boldsymbol{p}_{n}\right|_{2} > r_{\text{sen}} \end{cases}$$

(19)

where  $V_a^{m\to n}$  denotes the synthetic speed of AUV sailing from the grid m to the grid n, and  $\hat{V}_a^{m\to n} = V_a^{m\to n}/V_p$  denotes the  $V_a^{m\to n}$  normalized value. and velocity  $V_a$  satisfy the following equation

$$|\boldsymbol{V}_{a}|^{2} + |\boldsymbol{V}_{c}|^{2} - 2|\boldsymbol{V}_{a}||\boldsymbol{V}_{c}|\cos\langle\boldsymbol{V}_{a},\boldsymbol{V}_{c}\rangle = |\boldsymbol{V}_{p}|^{2}$$
(20)

where  $V_c$  is the velocity vector of the ocean current and  $V_p$  is the propulsive velocity vector of the AUV. Compared with the original formula, this formula takes into account the effect of ocean currents and uses the sailing time of neighboring grids to determine the connection weights between neurons instead of directly using the Euclidean distances of neighboring grids, which makes the algorithm more realistic.

In addition, in the traditional GBNN algorithm, the external stimulus relies only on the current position of the target and the surrounding obstacles for path planning. However, considering the complex changes that AUVs may encounter in dynamic environments, this study chooses to employ a confidence function to adjust the external stimulus matrix in real time, thus dynamically adjusting the path planning of AUVs. This approach enables the AUV not only to avoid obstacles effectively, but also to move towards the target quickly and efficiently.

The core formula of the confidence function is shown as follows

$$b_{m} = \xi \cdot (N_{m} + D_{m}) + G_{m}$$
(21)
$$N_{m} = \cos(\Delta \alpha)$$
(22)
$$D_{m} = e^{\frac{-|p_{i} - p_{m}|_{2}}{dist_{max}}}$$
(23)

where  $b_m$  denotes the set letter value of the grid m,  $N_m$  is a direction function that describes the angular relationship between the target and the current AUV and guides the AUV toward the target,  $\Delta \alpha$  is the angular difference between the target and the current

grid.  $D_{\rm m}$  is a distance function that gives an excitatory stimulus based on the distance between the grid m and the target, causing the AUV to choose the direction that is the shortest distance from the target,  $|p_t-p_m|_2$  is the distance between the target and the grid m, and  $dist_{\rm max}$  is a constant that controls the range of influence of the distance.  $G_m$  is an indicator function of whether the grid is occupied or not, and is set to -10 if the grid is occupied, and 0 otherwise.  $\xi$  is a constant used to weight the effects of and [13].

Then the neuron activity value function can be rewritten as follows

$$a_m^{t+1} = g(b_m^t + o(W_{m,n}^t, a_m^t))$$
(24)

where the set letter value  $b_m^t$  replaces the conventional external stimulus I,  $o(W_{m,n}^t, a_m^t)$  denoting the result after a  $3 \times 3 \times 3$  receptive field and a convolution with a step size of 1 is performed using the pair.

Global information about target escape in the network is propagated through the convolution operation in each iteration. An insufficient number of iterations may prevent the effective propagation of global information, while too much convolution leads to a significant increase in the computational complexity of the algorithm. The number of convolutions is calculated using a weighted average in conjunction with the judgment model of the Apollo circle as shown in the following equation.

$$n_{\text{cov}}^{t} = \max(\left|\frac{1}{\tau} \frac{\sum \left|\boldsymbol{A}_{a_{i}}, \boldsymbol{p}_{tar}\right|_{2} \cdot \left|\boldsymbol{p}_{a_{i}} - \boldsymbol{p}_{tar}\right|_{2}}{\sum \left|\boldsymbol{A}_{a_{i}}, \boldsymbol{p}_{tar}\right|_{2}}\right|, 1)$$

(25)

where  $n_{\text{cov}}^t$  denotes the number of convolutions at time t,  $\max(\square)$  is the maximum function,  $\lfloor \square \rfloor$  denotes the downward rounding function,  $\left| \boldsymbol{A}_{a_i}, \boldsymbol{p}_{tar} \right|_2$  denotes the Euclidean distance between the center of the Apollonius circle of the *i*-th AUV and the target,  $\left| \boldsymbol{p}_{a_i} - \boldsymbol{p}_{tar} \right|_2$  denotes the Euclidean distance between the location of the *i*-th AUV and the target, and  $\tau$  is the raster resolution.

Performing  $n_{con}$  convolution on the  $M_x \times M_y \times M_z$  image still has a high computational complexity, which can be reduced by processing o(x) as a global guide  $\hat{o}(x)$  if  $o(W_{m,n}^t, a_m^t)$  only used as a global guide and does not directly determine the shape of the trapping path.

First, an average pooling kernel of size  $s \times s \times s$  is used to perform a pooling operation on a' with step size s to extract the mean value of the inputs in each receptive field. Then, multiple convolution

operations are performed after calculating the number of convolutions, and the resolution of the grid becomes a multiple of the original resolution. Finally, the convolved image is resampled by a bicubic interpolation method to recover the element size. This operation is called Mean Pooling Multiple Convolution Resampling (MPMCR).

Observing the traditional GBNN update and MPMCR processes from a convolutional point of view, it can be easily seen that the traditional GBNN model can only propagate global information outward to a mesh during an update process. Compared with traditional GBNN, MPMCR can propagate global information to a farther network in one update process, improving the ability of IGBNN to jump out of the local optimum. In addition, the time complexity of MPMCR is as follows

$$O(\frac{27n_{\text{cov}}^t M_x \times M_y \times M_z}{s^3} + 2M_x \times M_y \times M_z)$$
 (26)

In contrast, the baseline method computes the dynamic output matrix via a single convolution with a  $3\times3\times3$  kernel, resulting in a time complexity of  $O(27M_x\times M_y\times M_z)$ . With the pooling kernel size set to s=5, the MPMCR method's time complexity is  $O((\frac{27n_{cov}^l}{125} + 2)M_x\times M_y\times M_z)$ . Compared to the baseline's time complexity  $O(27M_x\times M_y\times M_z)$ , the MPMCR method is less computationally intensive when  $n_{cov}^l < 115$ , Boundary analysis shows  $n_{cov}^l$  is an integer between 1 and 6, ensuring the MPMCR method's time complexity is always lower than the baseline.

However, MPMCR still needs to avoid the problem of easily falling into dead zones and resampling oversized elements in the result matrix  $E^{r}$  [29] Therefore, after each MPMCR, a normalization process should be performed, i.e., regularization.

$$\hat{\boldsymbol{E}}_{m}^{t} = \frac{\boldsymbol{E}_{m}^{t}}{\sum_{m}^{M} \boldsymbol{E}_{m}^{t}}$$

(27)

By combining the MPMCR and the processes included in the  $\hat{o}(\Box)$ , the formula for the neuronal activity value can be reconstructed as

$$a_m^{t+1} = g(b_m^t + \hat{o}(W_{m,n}^t, a_m^t, s))$$
28)

#### 2.3 Cooperation mechanisms

Unlike traditional allocation based solely on the distance between the pursuers and the target, this study takes the angle from each seiner to the marquee position into account along with the distance. The candidate positions were set as a total of 26 grid coordinates adjacent to the grid where the target was located, and when the three roundups simultaneously occupied three of these 26 grids and satisfied the

Apollonius circle's decision condition, the roundup was judged successful.

To ensure effective capture, this study employs the artificial potential field method [30] to guide pursuers toward optimal positions by adjusting their approach angles. In the pursuit process, the enclosure farthest from the target is the designated encloser, and its movement is realized by adjusting the direction of the combined force of the other two enclosers to ensure that the combined force of these two enclosers points in the direction of the designated encloser as much as possible, so as to effectively drive the target to the position of the designated encloser.

In the specific execution process, the applied force can be simply set as the unit vector of the candidate position pointing to the target position  $u_i$  and  $u_j$ , then the combined force is the sum of the two unit vectors, and the angle between the combined force and the direction of the designated fencer is as follows

$$FC_{total} = u_i + u_j$$
(29)
$$\varpi = \arccos(\frac{FC_{total} \cdot u_{rm}}{\|FC_{total}\| \cdot \|u_{rm}\|})$$
(30)

where  $u_{m}$  is the unit vector of the target pointing to the specified seiner

$$\boldsymbol{u}_{rm} = \frac{\boldsymbol{p}_{a_{rm}} - \boldsymbol{p}_{tar}}{\left\|\boldsymbol{p}_{a_{rm}} - \boldsymbol{p}_{tar}\right\|}$$

(31)

In addition, the total distance is the sum of the Euclidean distances between the enclosing AUV and its corresponding marquee position, then the objective function can be set as C

$$D_{a,mid} = \sum_{a=1}^{3} \left\| \boldsymbol{p}_{a} - \boldsymbol{p}_{a,mid} \right\|$$

$$(32)$$

$$C = (1 - e^{-t}) \cdot \frac{D_{a,mid}}{3 \cdot dist_{\text{max}}} + e^{-t} \cdot \frac{\varpi}{\pi}$$

$$(33)$$

where  $p_{a,mid}$  is the coordinate of the marquee position corresponding to the AUV,  $dist_{max}$  is the maximum size of the map, and  $e^{-t}$  is the time decay factor. The complete IEKF-IGBNN algorithm flow is shown below in Figure 3.

Based on this objective function, traversing all combinations of candidate locations and selecting the point pairs that minimize the objective function while satisfying the Apollonius circle decision condition, the target location, where the rounded-up AUV is heading to, can be determined.

#### III. RESULTS AND DISCUSSION

In this section, we first compare the improved algorithm in this paper with multiple baseline algorithms in the same environment where multiple obstacles are present to reveal the superiority of this algorithm in terms of roundup efficiency. Subsequently, we test the algorithm in environments with different obstacles and current distributions to verify the generalization ability of the algorithm. Finally, the anti-interference ability of the algorithm is further verified by testing under different sensor noise conditions.

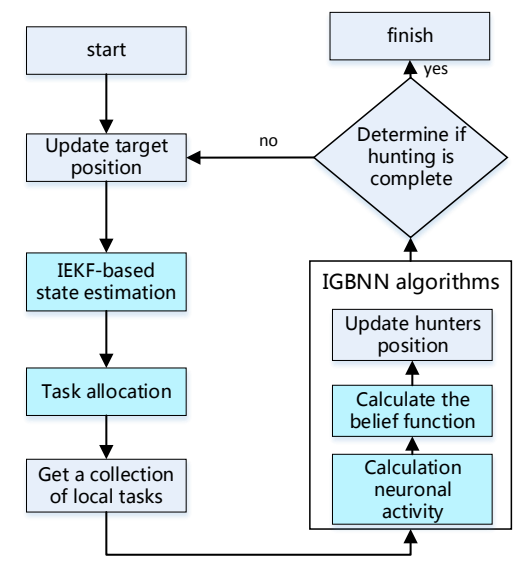


Figure 3. The running process of improving algorithm

### 1. Experimental setup

The experimental scene is a  $500 \times 500 \times 500$ m square region, which is finely divided into a  $50 \times 50 \times 50$  raster network with a resolution of 10m per grid, and four obstacles are randomly distributed in the region, whose *lengths*, widths, and heights are randomly generated from 10m to 100m, and the experiment-related parameters are shown in Table 1.

# 2.\_Algorithm validation

In order to prove the advantages of the IEKF-IGBNN algorithm, a series of roundup algorithms such as the original GBNN, GBNN-DIS, GBNN-RES, and GBNN-CBBA are selected as the control group. The simulation comparison of the roundup effect of all the above algorithms is carried out under the same experimental conditions, and the simulation results are shown in Table 2 and Fig. 4-Fig. 8.

TABLE 1 EXPERIMENTAL PARAMETER SETTINGS

notation	mean	value
$\tau / m$	Raster resolution	10
$\chi/m$	Vortex center coordinates	(500,0),(500,500),(250,150) (0,300),(100,550),(50,50)
Ω	vortex strength	-1,1,-1,1,1,-1
$r_{c}/m$	vortex radius	60,80,60,120,80,120

$v_a/(m/s)$	Propulsion speed	1
$V_a/(m/3)$	for hunters	1
$v_{tar}/(m/s)$	Propulsion speed	0.5
$V_{tar}/(m/S)$	for target	0.5
	Measurement of	
ρ	the scale factor of	0.99
	the noise matrix	
	Update factors for	
λ	process noise	0.1
	matrices	
δ	Smoothness	0.9
0	coefficient	0.9
	Connection	
$\eta$	weight decay	0.95
	factor	
	Transformation	
β	function decay	0.1
	factor	
$G_{\scriptscriptstyle m}$	Penalty for raster	10
$G_m$	m being occupied	-10
	Confidence	
ξ	function	0.6
-	weighting factor	
G	Mean pooling	5
S	kernel size	3

TABLE 2 IMPROVED ALGORITHM AND BENCHMARK ALGORITHM EXPERIMENTAL RESULTS

algorithm	Average distance of hunters	Average time of hunters
IEKF-IGBNN	451.6	516
GBNN_CBBA	547.2	649
GBNN_RES	545.5	626
GBNN_DIS	752.2	772
GBNN	1289.5	1457

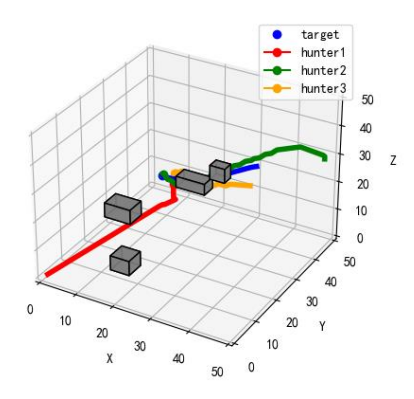


Figure 4. The running result of improving algorithm

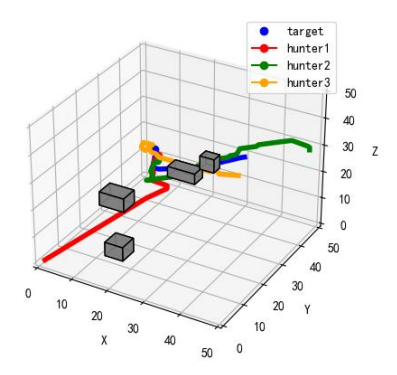


Figure 5. The running result of GBNN CBBA

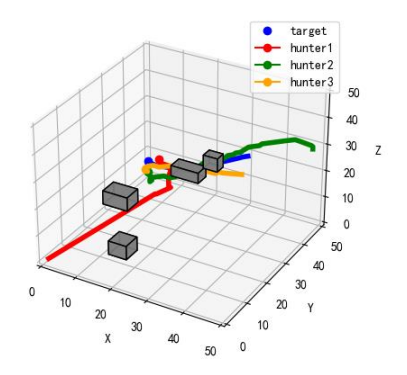


Figure 6. The running result of GBNN\_RES

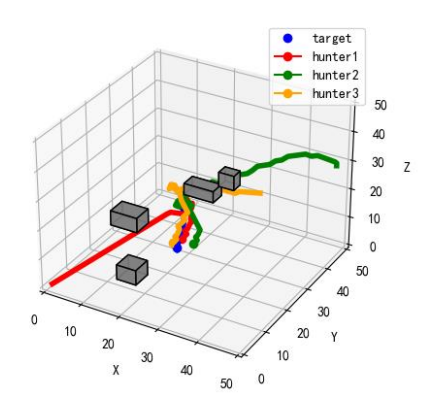


Figure 7. The running result of GBNN\_DIS

The experimental results show that the IEKF-IGBNN algorithm performs well in dynamic target capture tasks, with an average capture distance of 451.6 meters, which is superior to all other algorithms. Compared to the GBNN\_CBBA algorithm, this distance has been reduced by 17.5%; Compared with GBNN-RE, GBNN-DIS, and traditional GBNN algorithms, it has reduced by 17.2%, 40.0%, and 65.0%, respectively. In addition, the time step of IEKF-IGBNN is 516, which is also the shortest, reducing at least 17.6% compared to other algorithms and 64.6% compared to traditional GBNN. These results demonstrate significant advantages in distance and time efficiency of the improvement, demonstrating its efficiency and effectiveness in dynamic target capture tasks.

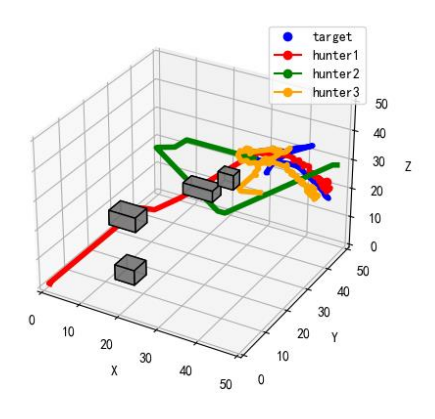


Figure 8. The running result of GBNN

#### 2. Verification of generalization capabilities

To verify the generalization ability of the improved algorithm, the overall map environment is altered by randomly adjusting the position, size, and number of obstacles within the map, as well as changing the strength and direction of ocean currents, and the experiment is repeated 50 times. During this process, the initial positions of the roundup AUVs and the target AUVs are kept constant to ensure the stability of the experimental conditions. The operation results of the improved algorithms and the various benchmark algorithms under 50 randomized experiments are shown in Tables 3 and 4 and Figures 9 and 10.

From Table 3, it can be analyzed that the improved algorithm has significant advantages over other algorithms in terms of total sailing distance. Compared to other algorithms, its average distance has decreased by 20.38% to 53.85%, with the optimization of traditional GBNN being particularly outstanding, reaching 53.85%. In the worst case, the maximum distance of IGBNN is 1706 meters, which is 25.34% to 59.33% lower than other algorithms; In the best-case scenario, its minimum distance is 1269 meters, which is 5.51% to 53.21% less than other algorithms. In addition, the data range of the improved algorithm is only 437 meters, far smaller than other algorithms.

From Table 4, it can be analyzed that the improved algorithm also outperforms the other algorithms in terms of time efficiency. Compared with other algorithms, its average navigation time has been optimized by 18.84% to 55.34%, the maximum navigation time is 27% to 60% lower than other algorithms, and the shortest navigation time has been reduced by 5% to 54.5%. It is superior to the benchmark algorithm in all dimensions, reflecting the superior performance of the improved algorithm in terms of capture efficiency and generalization ability.

TABLE 3 STATISTICAL RESULTS OF REPEATED EXPERIMENT DISTANCE

EXIERIMENT DISTANCE					
	Maximum	Minimum	Average		
	total	total	total		
algorithm	sailing	sailing	distance		
	distance	distance	traveled		
	(m)	(m)	(m)		
IEKF-IGBNN	1706	1269	1455		
GBNN_CBBA	3150	1632	2162		
GBNN_RES	2390	1400	1872		
GBNN_DIS	2285	1343	1827		
GBNN	4194	2712	3153		

TABLE 4 STATISTICAL RESULTS OF REPEATED EXPERIMENT TIME

algorithm	Maximum sailing time (steps)	Minimum sailing time (steps)	Average distance time (steps)
IEKF-IGBNN	629	496	552
GBNN_CBBA	1137	618	797
GBNN_RES	909	549	705
GBNN_DIS	862	522	680

GBNN	1581	1091	1237

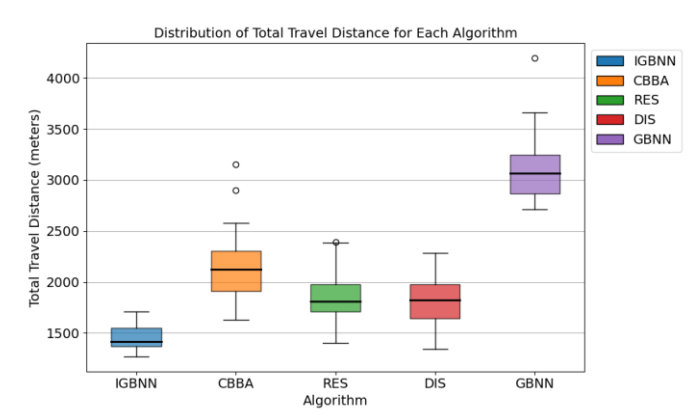


Figure 9. Box plot of total sailing distance distribution

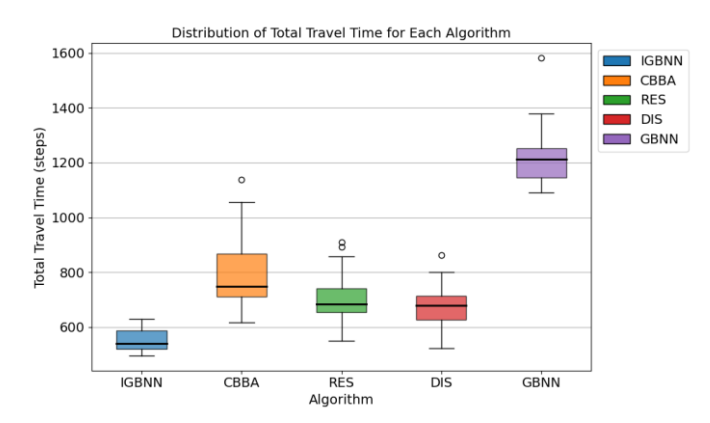


Figure 10. Box plot of sailing time distribution

From the box plot, it can also be seen that the improved algorithm has lower median, upper and lower quartiles than other algorithms in both distance and time, and its box size is smaller, indicating that its performance fluctuates less in different environments and has higher stability.

#### Anti interference capability verification

Due to the inherent positioning errors of sonar in underwater environments, research has shown that the current sonar ranging accuracy is usually within the range. Therefore, three simulation conditions are set: the mean distance measurement error is 5m, 10m, 15m, and 25m, respectively, and the distance measurement error variance is 1m2. The simulation experiments for each condition were repeated 20 times to verify and demonstrate the superior anti-interference ability of the algorithm. The experimental results are shown in Tables 5-6 and Figures 11-12.

TABLE 5 STATISTICS OF AVERAGE TOTAL DISTANCE TRAVELED UNDER DIFFERENT MEANS WITH A VARIANCE OF 1 M<sup>2</sup> IN SENSOR MEASUREMENT ERROR

	Mean	Mean	Mean	Mean
algorithm	error	error	error	error
	5m	10m	15m	25m
IEKF-IGBNN	1369	1407	1430	1513
GBNN_CBBA	1945	2171	2258	2344
GBNN_RES	1697	1730	2063	2462

GBNN_DIS	1924	1838	1801	2148
GBNN	3232	3046	3161	3715

TABLE 6 STATISTICS OF AVERAGE TRAVEL TIME
UNDER DIFFERENT MEANS WITH A
VARIANCE OF 1 M<sup>2</sup> IN SENSOR
MEASUREMENT ERROR

	Mean	Mean	Mean	Mean
algorithm	error	error	error	error
_	5m	10m	15m	25m
IEKF-IGBNN	531	541	551	573
GBNN_CBBA	730	732	839	883
GBNN_RES	731	653	774	932
GBNN_DIS	692	703	664	779
GBNN	1243	1182	1239	1424

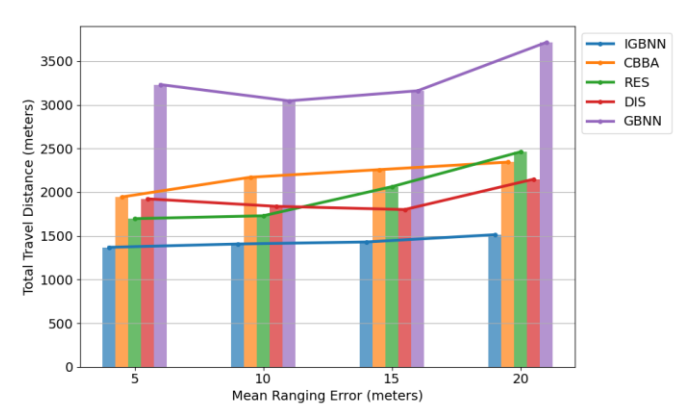


Figure 11. Bar chart of total sailing distance distribution

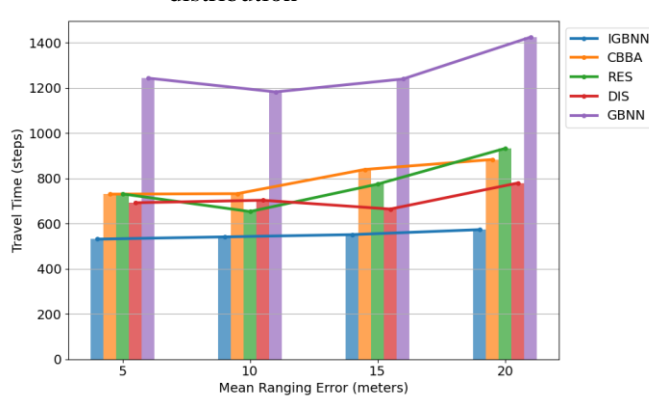


Figure 12. Bar chart of sailing time distribution

The improved algorithm achieved an average total distance of 1429.75 meters across sonar ranging errors from 5 to 25 meters, significantly outperforming other algorithms. Compared to the original GBNN, it has reduced the distance by an average of about 56.5%; Compared to GBNN\_CBBA, GBNN-RE, and GBNN-DIS, they decreased by approximately 34.4%, 28.1%, and 25.8%, respectively. Especially when the accuracy is low, the advantages of improving the algorithm are more obvious. In terms of navigation time, numerically speaking, the average navigation time of the improved algorithm is 549 steps, which is consistently more than 54.2% lower than GBNN under different sonar ranging errors, and 22.6% to 31.0% lower than other algorithms.

In addition, Experimental results demonstrate that the proposed algorithm achieves a total navigation distance

fluctuation range of 144 meters and a total navigation time fluctuation range of 42 steps, both indicating excellent stability. In contrast, the GBNN\_RES algorithm exhibits a navigation distance fluctuation range of 765 meters and a total navigation time of 279 steps, the poorest performance among all compared algorithms, highlighting its high sensitivity to measurement errors and lack of stability. Compared to other algorithms, the proposed method shows a significantly smaller fluctuation range, demonstrating that the IEKF effectively mitigates the impact of sonar detection errors, substantially reducing the influence of measurement inaccuracies and enhancing encirclement efficiency. In summary, the proposed algorithm exhibits outstanding stability and robustness against interference.

# 4. Validation of Adaptability in Strong Adversarial Ocean Current Environments

To rigorously validate the robustness of the improved algorithm under strong ocean current conditions, we conducted controlled experiments by fixing the positions of obstacles and AUVs while solely varying the intensity and direction of ocean currents to simulate diverse current environments. Four distinct current intensities (-2, -1, 1, 2) were selected, with positive values representing counterclockwise vortex rotation and negative values indicating clockwise rotation. Each intensity level was tested through 10 repeated experiments to ensure statistical reliability. The experimental results for the improved algorithm and baseline algorithms are presented in Tables 7-8 and Figures 13-14, comprehensively demonstrating the algorithms' performance across varying current intensities and directions.

TABLE 7 STATISTICS OF AVERAGE SAILING TIME UNDER DIFFERENT OCEAN CURRENT INTENSITIES

	Vortex	Vortex	Vortex	Vortex
algorithm	strength	strength	strength	strength
	-2	-1	1	2
IEKF-IGBNN	562	516	583	637
GBNN_CBBA	631	581	909	872
GBNN_RES	571	741	803	1072
GBNN_DIS	628	528	886	1071
GBNN	1195	1157	1252	1896

TABLE 8 STATISTICS OF AVERAGE TOTAL SAILING
DISTANCE UNDER DIFFERENT OCEAN
CURRENT INTENSITIES

	Vortex	Vortex	Vortex	Vortex
algorithm	strength	strength	strength	strength
	-2	-1	1	2
IEKF-IGBNN	1815	1720	1565	1724
GBNN_CBBA	2045	2361	2073	2543
GBNN_RES	1921	1751	2169	2863
GBNN_DIS	2222	1914	2338	2247
GBNN	3580	3440	2926	2991

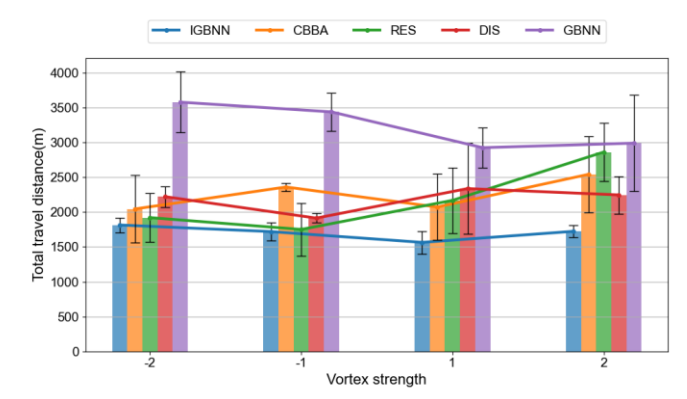


Figure 13. Distribution of Average Sailing Time under Different Ocean Current Intensities

**IEKF-IGBNN** The algorithm demonstrates exceptional performance in both sailing time and total sailing distance across varying ocean current intensities, showcasing significant superiority. In terms of travelling time, IEKF-IGBNN consistently achieves the lowest values, reducing sailing time by up to 66.4% compared to the baseline GBNN algorithm. Against other algorithms, IEKF-IGBNN outperforms in all vortex strength conditions, with particularly pronounced advantages under strong currents. Moreover, its sailing time exhibits minimal variation (121 time steps), far lower than GBNN and other variants, highlighting its remarkable stability and adaptability in dynamic marine environments.

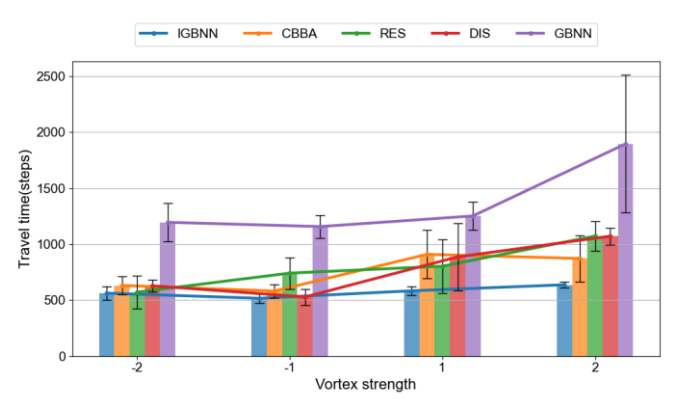


Figure 14. Distribution of Average Total Sailing
Distance under Different Ocean Current
Intensities

Regarding total sailing distance, IEKF-IGBNN consistently maintains the shortest distances, achieving reductions of 42.4% to 50.0% compared to the baseline GBNN. Compared to other algorithms, it saves 11.2% to 33.1% in distance across all conditions, with superior performance in strong current scenarios. Its distance variation is exceptionally small (250 meters), significantly less than GBNN and other variants, further underscoring its robustness. From the error bars in the figure, it is evident that the improved algorithm has significantly shorter error bars compared to other algorithms, demonstrating its higher stability and reliability.

In summary, the IEKF-IGBNN algorithm exhibits substantial advantages in optimizing both sailing time

and distance, delivering significant reductions while maintaining exceptional stability and adaptability across diverse vortex strengths. Compared to the baseline GBNN and other variants, IEKF-IGBNN excels in efficiency, robustness, and navigational planning in complex marine environments, making it the optimal choice.

#### IV. CONCLUSION

This study investigates dynamic target encirclement by multiple AUVs in 3D underwater environments. We developed an IEKF to address sonar detection errors, significantly enhancing target position prediction accuracy and system robustness. Furthermore, an optimized GBNN improves path planning efficiency through refined neuron activation and enhanced AUV collaboration. Simulations confirm the effectiveness and generalization of the proposed algorithms. However, the study is limited by the absence of physical experimental validation and its focus on single-target encirclement. research should prioritize real-world experimental validation, extend the framework to multitarget encirclement scenarios, and investigate distributed cooperative task allocation for swarm-based operations.

#### REFERENCES

- [1] LI L, LI Y P, WANG Y L, et al. Multi-AUV coverage path planning algorithm using side-scan sonar for maritime search[J]. Ocean Engineering, 2024, 300: 117396.
- [2] ZHANG Y X, WANG Q, SHEN Y, et al. Multi-AUV cooperative search method based on dynamic optimal coverage[J]. Ocean Engineering, 2023, 288: 116168.
- [3] YAO P, QIU L Y, QI J P, et al. AUV path planning for coverage search of static target in ocean environment[J]. Ocean Engineering, 2021, 241: 110050.
- [4] ZHANG Y X, LI Y P, LI S, et al. Multi-target tracking in underwater multistatic AUV networks with a robust Poisson Multi-Bernoulli filter[J]. Ocean Engineering, 2023, 284: 115167.
- [5] CUI J K, HOU M X, PENG Z, et al. Hamiltonian based AUV navigation using adaptive finite-time trajectory tracking control[J]. Ocean Engineering, 2025, 320: 120329.
- [6] GUO Y Y, QIN H D, XU B, et al. Composite learning adaptive sliding mode control for AUV target tracking[J]. Neurocomputing, 2019, 351: 180-186.
- [7] ZHAO Z Y, FENG X L, JIANG C, et al. Distributed short-term predictive control for AUV clusters in underwater cooperative hunting tasks[J]. Ocean Engineering, 2024, 301: 117343.
- [8] YU J B, CHEN Z H, ZHAO Z Y, et al. A cooperative hunting method for multi-USVs based on trajectory prediction by OR-LSTM [J].

- IEEE Transactions on Vehicular Technology,2024,73(12):18087-18101.
- [9] CAO Z Q, TAN M, LI L, et al. Cooperative hunting by distributed mobile robots based on local interaction[J]. IEEE Transactions on Robotics, 2006, 22(2): 402-406.
- [10] SUN Z Y, SUN H B, LI P, et al. Cooperative strategy for pursuit-evasion problem in the presence of static and dynamic obstacles[J]. Ocean engineering, 2023, 279: 114476.
- [11] CUI Y F, XU J, WEN X, et al. Anti-disturbance cooperative formation containment control for multiple autonomous underwater vehicles with actuator saturation[J]. Ocean Engineering, 2022, 266: 113026.
- [12] HU J Q, WU H S, ZHAN R J, et al. Self-organized search-attack mission planning for UAV swarm based on wolf pack hunting behavior[J]. Journal of systems engineering and electronics, 2021, 32(6): 1463-1476.
- [13] HUANG Z R, ZHU D Q, SUN B. A multi-AUV cooperative hunting method in 3-D underwater environment with obstacle[J]. Engineering Applications of Artificial Intelligence, 2016, 50: 192-200.
- [14] PENG Y, ZHAO Z Y. Improved Glasius bioinspired neural network for target search by multi-agents[J]. Information Sciences, 2021, 568: 40-53.
- [15] ZH;ANG A, WANG W H, BI W H, et al. A path planning method based on deep reinforcement learning for AUV in complex marine environment[J]. Ocean Engineering, 2024, 313: 119354.
- [16]Jiang Yong, Wang Linbo, Wang Mengyi, etc Collaborative capture strategy for high-speed and highly maneuverable targets based on coverage theory [J]. Journal of Engineering Science, 2024, 46 (07): 1169-1178
- [17] HUA X, LIU J, ZHANG J J, et al. An apollonius circle based game theory and Q-learning for cooperative hunting in unmanned aerial vehicle cluster[J]. Computers and Electrical Engineering, 2023, 110: 108876.
- [18] HASAN A, ASFIHANI T, OSEN O, et al. Leveraging digital twins for fault diagnosis in autonomous ships[J]. Ocean Engineering, 2024, 292: 116546.
- [19] Sheng Menggang, Lou Xing, Chen Yangzhuo, etc Research on EMA/EKF positioning algorithm based on optimal propagation path [J]. Navigation and Timing, 2022,9 (06): 141-149
- [20] MOHAMMAD M, NAIARI A, HOSSEYNZADEH M. Passive tracking of a target based on Supervisory adaptive EKF and CKF[C]//2020 IEEE 17th International Conference on Smart Communities: Improving

- Quality of Life Using ICT, IoT and AI (HONET). IEEE, 2020: 1-5.
- [21] AKHLAGHI S, ZHOU N, HUANG Z Y. Adaptive adjustment of noise covariance in Kalman filter for dynamic state estimation[C]//2017 IEEE power & energy society general meeting. IEEE, 2017: 1-5.
- [22] H. V. Do, Y. H. Kim, Y. S. Kwon, S. H. Kang, H. J. Kim and J. W. Song, "An Adaptive Approach based on Multi-State Constraint Kalman Filter for UAVs," [C]//2021 21st International Conference on Control, Automation and Systems (ICCAS), Jeju, Korea, Republic of, 2021, pp. 481-485
- [23] Yao P, Wu K, Lou Y. Path planning for multiple unmanned surface vehicles using Glasius bioinspired neural network with Hungarian algorithm[J]. IEEE Systems Journal, 2022, 17(3): 3906-3917.
- [24] Chen L, Jiang B, Liu Y, et al. Application of adaptive EKF in real-time orbit determination[J]. Journal of the Brazilian Society of Mechanical Sciences and Engineering, 2021, 43(4): 187.
- [25] Liu J, Chen H, Liu N. Effective Sage-Husa Kalman filter for SINS/Doppler/Platform compass integrated navigation system[C]//2016 IEEE Chinese Guidance, Navigation and Control Conference (CGNCC). IEEE, 2016: 541-546.
- [26] Yi L, Wan A Y S, Le A V, et al. Complete coverage path planning for reconfigurable omnidirectional mobile robots with varying width using gbnn (n)[J]. Expert Systems with Applications, 2023, 228: 120349.
- [27] Cao X, Sun H, Jan G E. Multi-AUV cooperative target search and tracking in unknown underwater environment[J]. Ocean Engineering, 2018, 150: 1-11.
- [28] Muthugala M A V J, Samarakoon S M B P, Elara M R. Toward energy-efficient online complete coverage path planning of a ship hull maintenance robot based on glasius bio-inspired neural network[J]. Expert systems with applications, 2022, 187: 115940.
- [29] Li Y, Huang Y, Zou Z, et al. Multi-AUV underwater static target search method based on consensus-based bundle algorithm and improved Glasius bio-inspired neural network[J]. Information Sciences, 2024, 673: 120684.
- [30] Wang Y, Li J, Zhao S, et al. Hybrid path planning for USV with kinematic constraints and COLREGS based on improved APF-RRT and DWA[J]. Ocean Engineering, 2025, 318: 120128.

#### **Authors**

Qian Sun received the B.Eng., M.Eng., and Ph.D. degrees from Harbin Engineering University, Harbin, China, in 2010, 2013, and 2016, respectively. He is an Associate Professor at the College of Information and Communication Engineering, Harbin Engineering University. His current research interests include integrated navigation and multisensor information fusion.

**Xingyu Zhou** received the B.Eng. degree from Harbin Engineering University, Harbin, China, in 2023. He is currently a M. Eng. candidate in Electronic Information with Harbin Engineering University. His current research interests include multi-agent systems.

Weiyang Zhao received the B.Eng. degree from North University of China, Taiyuan, China, in 2018. He is currently a M.Eng. candidate in Electronic Information at Harbin Engineering University, China. His current research interests include communication signal modulation and multi-agent systems.

**Xing Jian** received the B.Eng. degree from North University of China, Taiyuan, China, in 2023. He is currently a M.Eng. candidate in Electronic Information at Harbin Engineering University, China. His research interests include multi-agent systems and opportunistic signal localization.